

We are IntechOpen, the world's leading publisher of Open Access books Built by scientists, for scientists

4,800

Open access books available

122,000

International authors and editors

135M

Downloads

Our authors are among the

154

Countries delivered to

TOP 1%

most cited scientists

12.2%

Contributors from top 500 universities



WEB OF SCIENCE™

Selection of our books indexed in the Book Citation Index
in Web of Science™ Core Collection (BKCI)

Interested in publishing with us?
Contact book.department@intechopen.com

Numbers displayed above are based on latest data collected.
For more information visit www.intechopen.com



Thermoelectric Generator Using Passive Cooling

*Robert Dell, Michael Thomas Petralia, Ashish Pokharel
and Runar Unnthorsson*

Abstract

This chapter presents an analysis of a point-of-use thermoelectric generator that is patented by one of the authors. The design, implementation and performance of the generator for powering electronic monitoring devices and charging batteries is discussed. This passive generator has no moving parts and relies on ambient air cooling. In one iteration it produces 6.9 W of steady state power using six Laird thermoelectric modules (Laird PB23 Series, HT8, 12) when placed on a 160°C steam pipe with a 30°C ambient environment (ΔT of 130°C). The generator produced 31.2 volts (V) open circuit and 0.89 amperes (A) short circuit. It successfully powered two microcontroller-based security cameras, one with a wireless Local Area Network (LAN) and another with cellular connectivity. In another scenario, the generator produced approximately 6 W with a steam pipe temperature of 140°C and an ambient of 25°C (ΔT of 115°C). This second system powered LED lights, a cellular-interfaced video surveillance system, and monitoring robots, while simultaneously trickle charging batteries. A third installation totally powered a stand-alone 3G web security camera system.

Keywords: thermoelectric generator, passive cooling, low temperature, waste-heat, point of use DC generator, thermoelectric module, steam pipe

1. Introduction

Internal temperature differences in almost all materials cause energetic excitation and the bulk motion of free electrons. This creates an electromotive force called the thermoelectric effect. Metals typically generate a few microvolts per degree Kelvin. Semiconductors can increase this rate by several orders of magnitude [1, 2].

The thermoelectric effect was reported in the mid-eighteenth century by Franz Ulrich Theodor Aepinus in his study of the mineral tourmaline [3–5]. In 1794, Alessandro Volta reported muscle spasms in a live frog's leg that were caused by two non-ferrous wires immersed in separate glasses of water. The glasses were connected by a partially immersed iron rod that had one end preheated in boiling water [5–7]. The generation of an electromotive force produced by heating the junction between two dissimilar metals came to be known as the Seebeck effect, in honor of Thomas Johann Seebeck, who is credited with the discovery of thermoelectric effects through his experiments in the 1820s [1, 8–13]. Later, in 1834, Jean Charles Athanase Peltier published an article on the inverse effect: temperature

anomalies observed near the boundary between two different conductors when a current is passed through them [1, 14]. William Thomson (eventually given the title Baron Kelvin) laid out a thermodynamic basis for thermoelectricity [15] using Joule's law of the electrical generation of heat in a homogeneous metallic conductor.

Continual advances in fundamental physics, materials science, heat transfer, electrical conductivity, and electromotive force-generating capability of thermoelectric materials [2, 16–20] have enabled the development of modern solid-state devices that can directly convert thermal energy to electrical energy. One notable application is in waste heat recovery systems [21, 22]. In 2017, the energy consumption for the United States of America was estimated by the Lawrence Livermore National Laboratory and the U.S. Department of Energy to be 9.77×10^{16} BTU (1.03×10^{20} J). Approximately 68% of this energy was classified as rejected (i.e., wasted) [23]. It is likely that most of the rejected energy was in the form of heat, thermal energy that is transferred between two systems by virtue of a temperature difference [24].

Waste thermal energy is not typically harvested due to its low energy potential. From a thermodynamic perspective, systems with small temperature differences have a low efficiency [25]. Frictional, gravitational, atmospheric, and elastic forces become significant. The resultant basic economics severely limit viable implementations.

Thermoelectric power generation systems can be robust with a relatively simple construction. Despite the low energy potentials of waste heat scenarios and low thermoelectric system efficiencies, they can be an ideal solution in low power applications that have limited electrical grid access and require low maintenance.

2. Background summary

Thermoelectric power generation systems (TEGs) are classical thermodynamic heat engines with no internal moving mechanical parts. An electromotive force is generated through the motion of the Fermi gas of electrons inside conductors and semiconductors (analogous to the molecular gas employed in a steam engine) [26]. A temperature gradient (∇T) induces this electric potential difference or voltage gradient (∇V) in a phenomenon known as either the thermoelectric, Seebeck, or Peltier effect. In general, the bulk material property called the Seebeck coefficient (α), governs thermoelectric behavior. This relationship can be expressed as: $\nabla V = \alpha \nabla T$. The electrochemical phenomenon is an electromotive force induced when two dissimilar metals are connected to form junctions maintained at different temperatures that generates electricity. Individual thermocouples are used to measure temperature when the amount of electricity generated is calibrated to correspond to the temperature. In TEGs, multiple thermocouples called thermoelectric modules (TEMs) are connected in series to generate higher voltages.

TEMs are essentially solid-state devices that convert heat flux into electrical energy. Commercially available TEMs often have more than one hundred thermocouples with pairs of *p*- and *n*-type semiconductors connected in series electrically. They are referred to as thermopiles. The thermopiles are typically sandwiched between two thin ceramic plates providing a platform to make both the electrical junctions and thermal interfaces. Two wires at the ends of the thermopile serve as the electrical connections for the TEM. If the opposing sides of the ceramic plates are maintained at different temperatures, direct current (DC) will be generated when the wires are connected to create a circuit. A simple TEG therefore consists of TEMs, a circuit load, a high-temperature heat transfer system (hot block), and a low-temperature heat transfer system (cold block). The two heat transfer systems are required to maintain the temperature difference between both sides of the TEM.

When electricity is added to a TEM, heat is moved from one ceramic surface to the other, which renders the TEM in its traditional role as a solid-state heat pump.

3. Generator system description

The authors have designed and patented a TEG that relies solely on passive cooling; i.e., natural conduction [27]. It can be easily mounted onto an existing pipe heat source.

Figure 1 shows 3D CAD models of the generator. It consists of a pair of mirrored assemblies. Each assembly has a hot block transition that doubles as a surface geometry adapter for three thermoelectric modules that are wired in series, and a cold block with a finned heat pipe [28].

The hot block transfers the heat from the pipe to the TEMs and the cold block removes the heat. The resultant temperature difference between the hot and cold blocks produces thermoelectric power when TEMs are sandwiched in between them. Multiple TEMs in a thermoelectric generator can boost the voltage when wired in series and the amperage when wired in parallel. The generator has a fast reaction; e.g., changes in airflow are almost immediately manifested in measurable voltage and amperage fluctuations.

The remainder of this section will describe in detail the generator's components, the generator's assembly and the setup of experiments carried out to test the design.

3.1 Heat source

Steel steam and hot water pipes in Iceland and New York City were used as test beds [28]. The steam and hot water pipes have internal temperatures between 85 and 160°C. The nominal dimensions of the pipe diameters used by the authors range from 1 to 3.5 in. Exterior and interior locations are used with preexisting and new dedicated pipes. In Iceland direct borehole lines and municipal geothermal hot water heat sources are used. In New York City, Consolidated Edison municipal steam lines were used for three early test configurations. A dedicated steam experimental test bed was developed at the Center for Innovation and Applied Technology at The Cooper Union for the Advancement of Science and Art.

The experimental test bed as shown on the left in **Figure 2** has an ESG Corporation 240-volt 3 phase SPEEDYELECTRIC 15A-2 electrode steam generator with a BFCR-404 automatic water feed pump and condensate return system. It has a

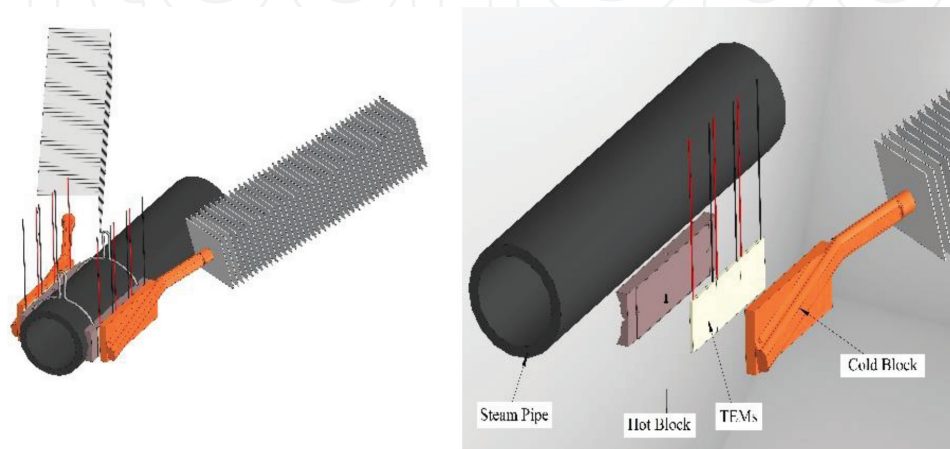


Figure 1.
3D CAD models of the thermoelectric generator assembled as a mirrored unit of two generators (left) and a schematic (right).



Figure 2. The test beds at The Cooper Union in New York City (left) and the Agricultural University of Iceland in Hveragerdi (right).

Parameter	Value
Internal pipe temperatures	85–160°C
Steam pipe thickness	0.19 in
Steam pipe outer diameter	1–3.5 in
Operating pressure	80–100 psig
Reservoir volume	30 gal

Table 1. Test bed heat source parameters.

30-gallon water reservoir and the condensate is bled manually. The system operating pressure was set at a maximum pressure of 100 psig and an 80 psig minimum when the unit automatically powered the electrodes until a maximum pressure was again obtained. The steel pipes have 2-in diameter pipes with a 1-in top pipe in a closed loop configuration. The thermoelectric generator is mounted on the bottom 2-in pipe.

The parameters for the heat source in the test bed are listed in **Table 1**. Shown on the right of **Figure 2**, at the Agricultural University of Iceland in Hveragerdi, the thermoelectric generators were attached outdoors to a geothermal steam borehole line. The generators were placed in adjoining protective sheds and attached to an old galvanized pipe with a temperature of between 100 and 140°C.

3.2 Hot block

The hot block creates a thermal channel to the TEMs. Although the hot block material should be chosen to maximize thermal conductivity, non-ferrous metals were not initially selected to prevent potential galvanic reactions between the hot block and the steel pipes. Steel hot blocks would also have the additional advantage of having the same rates of thermal contraction and expansion as the pipes, which helps to maintain the integrity of the thermal grease interfaces.

The hot block also has to accommodate a round steam pipe and a flat TEM, so the hot block is curved on one side and flat on the opposite side, seen in **Figure 3**.

Parallel lateral grooves were milled on the curved side of the hot block. This helped mitigate any differences in radius between the hot block and the steam pipe while also minimizing potential hot block warp. Warping of the hot block would

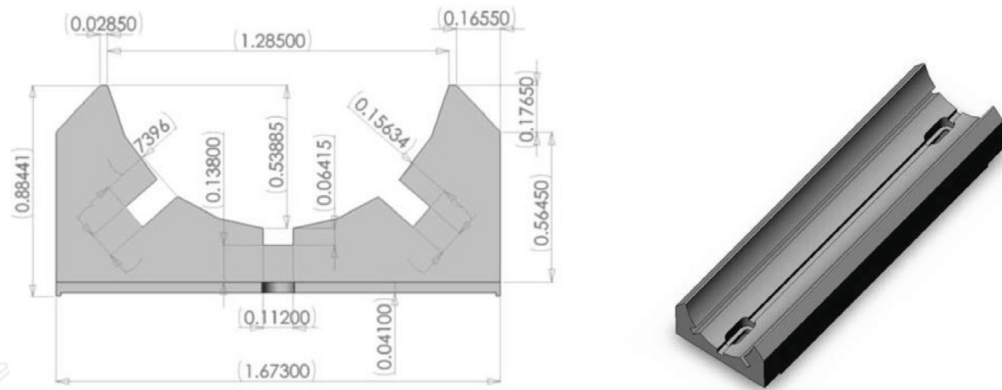


Figure 3.
 Cross section with dimensions in inches (left) and 3D rendering of the hot block (right).

Parameter	Value
Average block thickness	0.68 in
Block/module contact area	6.8 in ²
Pipe contact area	7.0 in ²
Number of grooves	3

Table 2.
 Hot block design parameters.

degrade the thermal integrity of the interfaces, and possibly damage the TEMs. A third function of the grooves is to expel excess thermal grease.

On the flat side of the authors' hot block, recesses were milled leaving slightly raised lateral flat rails on the edges. This forms a channel for the TEMs, which are slid into a precise controlled position with thermal grease between the surfaces. In traditional TEM installations without the recess and rails, the thermal grease inhibits precise positioning due to its lubricity.

The design parameters for the hot block are listed in **Table 2**.

3.3 Thermoelectric modules

The TEM used are tolerance lapped. They vary no more than 0.005 in. The surface area of contact with the hot and the cold blocks is approximately 1.5 in². Each mirrored side of the TEG has three TEMs in contact with the hot block, for a total of six TEMs wired in series for power production. ThermaTEC modules (Laird PB23 Series, HT8, 12) were designed to function in the higher temperature ranges of steam systems. Earlier versions of the TEG used Melcor model HT-4-12-40 modules, which provided lower amperage and higher voltage. Both modules meet or exceed current U.S. military specifications.

The design parameters for the module array are listed in **Table 3**.

3.4 Cold block

The cold block system was fabricated by Noren Products. The system consists of two mirrored heat pipes that are splayed back along the steam pipe. This increases the available space near the steam pipe. The geometry is important for safety concerns, and it enables installation in a one-foot radius envelope around the steam pipe. An added advantage is that the natural convection current around the steam pipe accelerates the cooling.

Parameter	Value
Number of modules	3
Seebeck coefficient	0.050 V/K
Thermal conductance	0.54 W/K
Module side dimension	1.5 in

Table 3.
Thermoelectric module array design parameters.

Parameter	Value
Fin thickness	0.02 in (aluminum) 0.03 in (copper)
Fin length	3–4 in
Fin spacing	0.25 in
Heat pipe outer diameter	0.66 in
Number of fins	41

Table 4.
Cold block design parameters for initial unit.

The main function of the cold block system is to provide a thermal channel between the cold plate of the thermoelectric module array and the ambient environment. The authors' thermoelectric generator is cooled passively by the ambient air. Cold blocks and their usual array of fins are sometimes referred to as “heat sinks”. In a larger thermal sense, they are only conduits to the heat sink, which is actually the immediate environment. This can be an outdoor setting or a confined space, such as a steam room, where an additional thermal analysis is needed for an accurate design assessment. The authors' cold block system consists of a thick milled copper plate, in direct contact to the TEM array. It is soldered to a copper heat pipe with attached square aluminum fins.

The design parameters for the cold block are listed in **Table 4**.

3.4.1 Heat pipe

Heat pipes are essentially heat siphons that rely on fluid phase change to greatly increase their heat transfer ability. They are different from traditional heat siphons, such as single pipe steam heating systems, because they have a porous layer next to the pipe's surface that accelerates the liquid flow by using capillary action caused by the increased surface area. There is often a smaller concentric internal pipe that serves as a dedicated return line.

Heat pipe transmission rates in terms of watts per unit area are more than 50 times greater than copper [29]. The internal fluid flow of the heat pipe relies in part on gravity, and it performs poorly if placed horizontally. A mild angle (e.g., 15 degrees from horizontal) is sufficient for the heat pipe chosen.

Heat pipes are also lightweight, weighing about one-fifth of traditional pipes for the same cooling effectiveness. A traditional heat pipe may create substantial stress on the TEMs due to the cantilevered weight. Heat pipes are also somewhat flexible.

3.4.2 Fins

Rectangular fins are mounted onto the heat pipe with a heat shrink fit. The system chosen relies primarily on natural convection, and a restriction on the fins is

that they must be nearly vertical to allow the flow to accelerate vertically between them. The spacing must also be sufficiently large that there is minimal interference between the thermal boundary layers of adjacent fins.

There are forty-one fins on each heat pipe assembly. They were 3 and 4 in². The output voltage is predicted to increase with increasing numbers of fins due to the increase in surface area, but there are diminishing returns. Doubling the number of fins to 82 (and lengthening the heat pipe to maintain the proper spacing) results in a modest 22% increase in output volt predicted (18.1–22.1 V), as can be seen in **Figure 4**. The longer heat pipe would also double the weight and be more unwieldy than the design chosen. The loss of robustness was determined to be more important than the projected power increase. Improvements in performance were achieved by increasing the fin dimension L . With 4-in fins, the output voltage was increased by 16%, the modification representing an 87% increase in surface area.

As expected, there is a slightly higher voltage for copper compared with aluminum fins. Copper has nearly double the thermal conductivity of aluminum, and the copper fins have a larger thickness in the prototype (0.02 in for aluminum and 0.03 in for copper). However, the difference is small because the fins are effectively thermally short. That is, the characteristic fin lengths are 13 and 7.5 in for copper and aluminum, respectively, whereas the fin dimension was only 3 in, less than half the characteristic lengths, so the temperature drop along the fin surface is small.

The natural convection coefficient increases with the decreasing vertical dimensions of the fins. Therefore, another means of improving performance (for thermally short fins) would be to use rectangular, rather than square, fins. For example, under these conditions, the convection coefficient is 5.9 W/m² °C for 3-in fins and 7.2 W/m² °C for 2-in fins. The predicted output voltage increases from 18.4 to 19.5 V if fins of 2 in (vertical) by 4.5 in are used, a 6.0% increase without increasing the fin area.

3.5 Thermal grease

Thermal greases can be employed to increase the thermal conductivity of the thermal interfaces. Traditional thermal greases are not recommended by the manufacturers for the applications described herein as they quickly dry at steam temperatures. A specifically modified version of the Ambrosia HT high-temperature

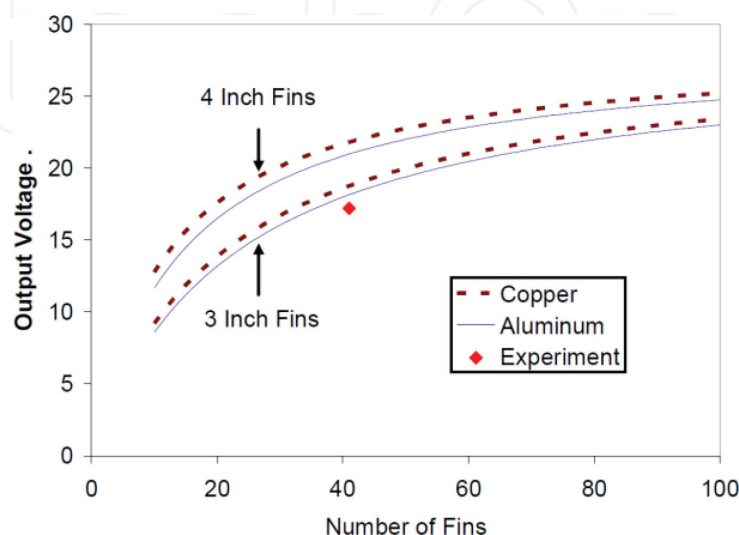


Figure 4. System open-circuit voltage as a function of the number of fins for copper and aluminum fins of 3-in (used in the prototype) and 4-in dimension. Experimental point and theoretical predictions are obtained from a pair of thermoelectric assemblies.



Figure 5.
CAD rendering of a pair of hot blocks connected by 2 cradles which act as springs and apply a clamping force.

thermal grease from Arctic Silver was employed. It contains nanoparticles that settle into any material voids over a period of approximately 100 h, thereby potentially increasing the system power. Later installations used Timtronics Red Ice thermal grease.

The thermal grease also doubles as a galvanic corrosion barrier between the dissimilar metals.

3.6 Clamping system

Clamps provide the pressure needed for basic attachment and to maintain the integrity of the thermal interfaces. A double wire spring connects the mirrored hot blocks in a cradle configuration for alignment and initial positioning purposes. Additionally, this cradle system serves as gripping points during installation and a connection point for the wire harnesses. A CAD rendering of the wire spring clamp and the hot blocks is shown in **Figure 5**.

3.7 Electrical energy storage

Batteries are traditionally used to store electrical energy for later use. In thermoelectric applications, a battery system can provide peak power. It also eliminates the inherent electrical noise that can interfere with the solid-state telemetry systems. Rechargeable lead-acid, NiCad, lithium-ion, or other battery storage can be used.

4. Theoretical considerations

4.1 Thermoelectric power

The theoretical power generated can be derived by modeling a TEM as a voltage source (V_o) with an internal resistance (r_i) and a circuit load resistance (r_L). If the module is short circuited (closed, with zero load resistance) the maximum electric current (I_c) is developed from the open circuit voltage with only the TEM's internal resistance. The short circuit current is given by Ohm's law: $I_c = V_o/r_i$. When an electrical load is placed across the module, the circuit current is decreased due to the

additional series resistance. The loaded circuit current is given by $I_L = V_o / (r_i + r_L)$. Here Ohm's law can be employed again, this time to determine the voltage across the load:

$$V_L = \left(\frac{r_L}{r_i + r_L} \right) V_o. \quad (1)$$

Since power is the energy output over time, voltage is the potential energy per electric charge, and current is the electric charge flow over time, the power available at the load of an electric circuit is given by $P_L = V_L I_L$. Thus, the power generated by a TEM can be expressed as

$$P_L = \left[\frac{r_L}{(r_i + r_L)^2} \right] V_o^2. \quad (2)$$

By solving $dP_L/dr_L = 0$, the maximum power is determined to occur when $r_L = r_i$, which is the classic case of impedance matching. The maximum power achievable can thus be written in terms of the open circuit voltage and the short circuit current:

$$P_{L, \max} = \frac{V_o I_c}{4}. \quad (3)$$

TEMs have multiple thermocouples connected in series and thermally in parallel. The plates on either side of the thermopile are at T_h and T_c . The power generated by the TEM can be expressed as

$$P_L = \left[\frac{r_L}{(r_i + r_L)^2} \right] \alpha^2 (T_h - T_c)^2. \quad (4)$$

4.2 Thermal resistance modeling

Thermal resistance is analogous to electrical resistance. The total resistance of a thermal circuit is therefore the cumulative total of the individual thermal resistors [30]. Overall system efficiency can be increased by lowering these thermal resistances. TEMs are placed between the hot and the cold blocks. Any other thermal connection would tend to reduce the change in temperature (ΔT) across the TEMs, which degrades the generated power.

The cold block's copper plate and the attached heat pipe are very thermally conductive when compared to the steel hot block and the TEM array. It can be regarded as de minimus, and therefore it is not included in the simplified analytical model. The thermal resistance associated with the connection of the heat pipe to the aluminum fins is also de minimus due to the minimal area of interface.

The base of each fin's contact with the heat pipe is maintained at the temperature of the cold side of the TEM.

4.2.1 Hot block

The heat source is the pipe. The heat flows from the pipe fluid to the inner surface of the steam pipe, the pipe wall, and a thermal grease interface. This connects to the hot block, another thermal grease interface and then to the hot side of the TEM.

The hot block system, R_H , consists mainly of three resistances in series:

$$R_H = R_{steam} + R_{pipe}(+R_{contact\ 1}) + R_{hotblock}(+R_{contact\ 2}). \quad (5)$$

The two contact resistances (thermal grease) shown in parentheses, between the steam pipe and the hot block, and between the hot block and the TEM, can be considered negligible if good thermal contact is maintained using an efficient thermal grease.

The thermal resistance between the steam and the pipe inner wall, R_{steam} , is a convective resistance and is approximated by

$$R_{steam} = \frac{1}{h_s A_s} \quad (6)$$

where A_s is the effective surface area and h_s is the convective coefficient of the condensing steam on the inside of the pipe wall. A_s will be somewhat larger than the contact area of the hot block due to three-dimensional effects.

The thermal resistance across the pipe wall is a conductive resistance and is approximated by:

$$R_{pipe} = \frac{t_p}{k_p A_p} \quad (7)$$

where A_p is the effective conductive area, k_p is the thermal conductivity, and t_p is the thickness of the pipe wall. A_p will again be somewhat larger than the contact area of the hot block due to three-dimensional effects.

The thermal resistance across the hot block is also a conductive resistance that is approximated by:

$$R_{hotblock} = \frac{t_{hb}}{k_{hb} A_{hb}} \quad (8)$$

where A_{hb} is taken to be the average area of the two contact surfaces of the hot block, k_{hb} is the thermal conductivity of the hot block, and t_{hb} is the average thickness of the block.

The total thermal resistance of the hot block system is thus approximated by

$$R_H = \frac{1}{h_s A_s} + \frac{t_p}{k_p A_p} + \frac{t_{hb}}{k_{hb} A_{hb}} \quad (9)$$

Note that approximately half of the thermal resistance is due to the hot block itself and the other half is due to a combination of condensation and conduction through the pipe wall. That is, the thermal resistance added with the hot block is comparable to the inherent thermal resistance of the existing pipe.

4.2.2 TEMs

The TEMs are thermally connected in parallel, so the thermal resistance for three modules is:

$$\frac{1}{R_{TEM}} = \frac{1}{R_{m,1}} + \frac{1}{R_{m,2}} + \frac{1}{R_{m,3}} \quad (10)$$

where $R_{m,i}$ is the thermal resistance of the i th TEM. Assuming all the TEMs have the same thermal resistance, R_m , this simplifies to:

$$R_{TEM} = \frac{R_m}{3}. \quad (11)$$

The thermal conductance of each module is taken to be 0.5 W/°C at 100°C. (The thermal conductance the inverse of the thermal resistance.) The thermal resistance of the three-TEM array is:

$$R_{TEM} = \frac{\frac{1}{0.5} \text{ C/W}}{3} = 0.67 \text{ C/W}. \quad (12)$$

4.2.3 Cold block

A simplified model of the cold block can be represented by a system of essentially parallel resistances. The cold block resistance, R_C , for N fins becomes:

$$\frac{1}{R_C} = \frac{1}{R_1} + \frac{1}{R_2} + \frac{1}{R_3} + \dots + \frac{1}{R_{N-1}} + \frac{1}{R_N}. \quad (13)$$

Assuming all the thermal resistances of the fins are equal ($R_1 = R_2 = R_3 = \dots = R_{N-1} = R_N = R_{fin}$), the system reduces to:

$$R_C = \frac{R_{fin}}{N}. \quad (14)$$

An estimate of the thermal resistance of the individual fins can be modeled as two thermal resistors in series:

$$R_{fin} = R_k + R_h. \quad (15)$$

where R_k is the thermal resistance associated thermal conduction within the fin material from the base toward the outer perimeter, and R_h is the thermal resistance associated with heat being transferred from the fin to the ambient air.

5. Results

The first test bed at The Cooper Union in New York City had a 3 in diameter steam pipe and ambient air temperatures of approximately 350°F (177°C) and 122°F (50°C), respectively. The ΔT was approximately 120°C. For the initial prototype, the first assembly had copper fins and the second had aluminum fins. The prototype had a voltage of 17.2 V, compared with the theoretical prediction of 18.4 V, which was the average of the 18.1 V predicted for aluminum and 18.8 V predicted for copper. These results demonstrate the output open circuit voltage, not how the system responds to an electrical load (with current being drawn). Therefore, the system voltage and current were also measured when the system was used to drive two different light bulbs. The closed circuit current (zero voltage) was found to be 0.70 A. A linear relationship was found experimentally to be

$$V = -24.4I + 17.2 \quad (16)$$

With the first assembly constructed with copper fins and the second with aluminum fins, the direct current system produced 17.2 V (open circuit) and 0.7 A (closed circuit). A theoretical methodology for predicting the output electrical power from an array of thermoelectric modules is developed and applied to this system.

As can be seen in **Figure 4**, the theoretical system output and the output was found to be extremely stable overtime. The theoretical model can therefore be used to predict the effect of changes in design parameters or operating conditions.

The output was found to be extremely stable over time.

The third assembly was constructed and tested to determine whether a heat pipe was necessary. The 16 mm heat pipe was replaced with a 38 mm solid copper rod manufactured by Noren Products and the fin size was adjusted so the system would yield comparable results to the first two assemblies. The theoretical model was extended to include the thermal resistance of this rod (which was assumed to be zero for the heat pipe). The solid copper rod weighs approximately 6 kg, as compared to 1.5 kg for the heat pipe. The solid copper assembly demanded considerable extra fabrication costs due to extensive welding, soldering, and extra machining.

The fourth design iteration increased the fin size from 3 to 4 in. The output increased from 8.18 to 11.54 V (a 40% increase). The experimental output of this fourth assembly was 14% higher than theoretically predicted. The third and fourth assemblies can be compared to note the effect of the heat pipe over the solid copper rod because both had 4-in fins.

The fifth and sixth assemblies tested were fit to a 1-in steam pipe at a Consolidated Edison facility in New York City. They were otherwise designed identically to the fourth assembly, with 4-in fins and a heat pipe. The fifth assembly contained three TEMs and had a measured open circuit voltage of 15.9 V, while the sixth only contained 2 TEMs and had a measured open circuit voltage of 12.1 V. These two assemblies provided uninterrupted power for at least 2 years.

Three assemblies were eventually moved to an outdoor location in Hveragerði, Iceland at the University of Iceland, where they were fit onto old galvanized pipes with surface temperatures of approximately 140°C from a geothermal steam bore-hole line. The steam pipe has been a reliable power source for almost 10 years. The total voltage of the three units in series after 9 months of exterior exposure was 39.2 V (open circuit) and the amperage was 0.64 (short circuit). The output in parallel was 13.4 V (open circuit) and 1.81 A (short circuit). The power produced was approximately 6W.

The TEMs were replaced and the new Timtronics Red Ice thermal grease was applied. In the winter of 2019 with a ΔT of 140°C, the open circuit voltage and short circuit current of the three assemblies were each measured independently in steady state, as is shown in **Table 5**. When the assemblies are wired in series, the voltages sum to 31.6 V and the power is approximately 10.7 W. The power generated by the TEGs was 257 Wh per day. **Figure 6** shows the total energy drawn from the TEGs. The energy drawn was 61 Wh per day. The entire 3G web camera system and its controls consume only 25% of the total power generated. In 2019 the test bed at the Center for Innovation and Applied Technology at The Cooper Union had steady-state open circuit voltage and short circuit current measuring 19.32 V and 0.96 A. The experimental data is represented in **Figure 7**. The maximum power

Assembly name	Voltage	Current
Generator 1	10.17 V	1.35 A
Generator 2	10.63 V	1.35 A
Generator 3	10.79 V	1.36 A

Table 5.
January 2019 Hveragerdi steady state voltage and amperage readings.



Figure 6. January 24 to February 21, 2019 3G system power consumption. The February 21 reading is less due to the time of day the readings were taken.

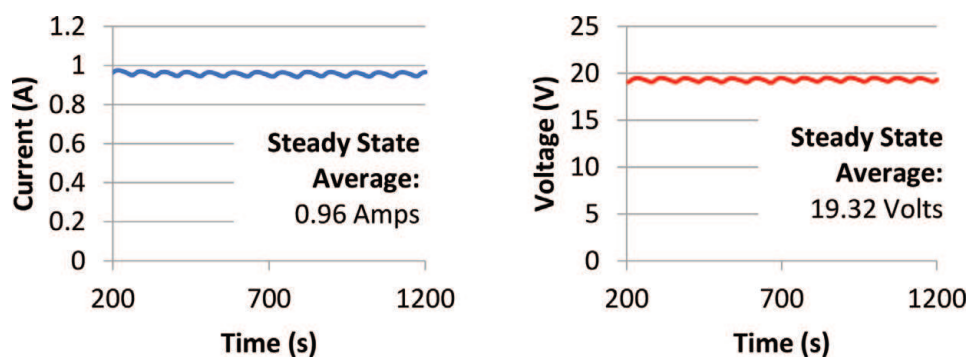


Figure 7. Experimental electrical power generation data from the New York City test bed recorded in January 2019. There is a steady-state average short-circuit current of 0.96 A (left) and a steady-state average open-circuit voltage of 19.32 V (right).

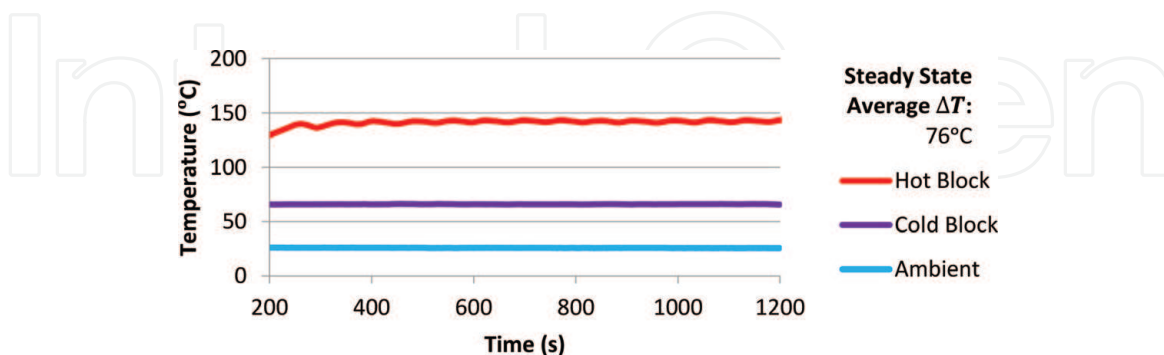


Figure 8. Experimental temperature difference (ΔT) data from the New York City test bed recorded in January 2019. There is a steady-state temperature difference of 76°C.

available, then, is 4.6 W. The hot block, cold block, and ambient temperatures were 142, 66, and 27°C, respectively. The experimental data is represented in **Figure 8**.

Figure 9 illustrates the linear voltage-ampereage of The Cooper Union thermoelectric generator. A Fluke 289 graphical multimeter using Flukeview software was used to record all of the measurements.

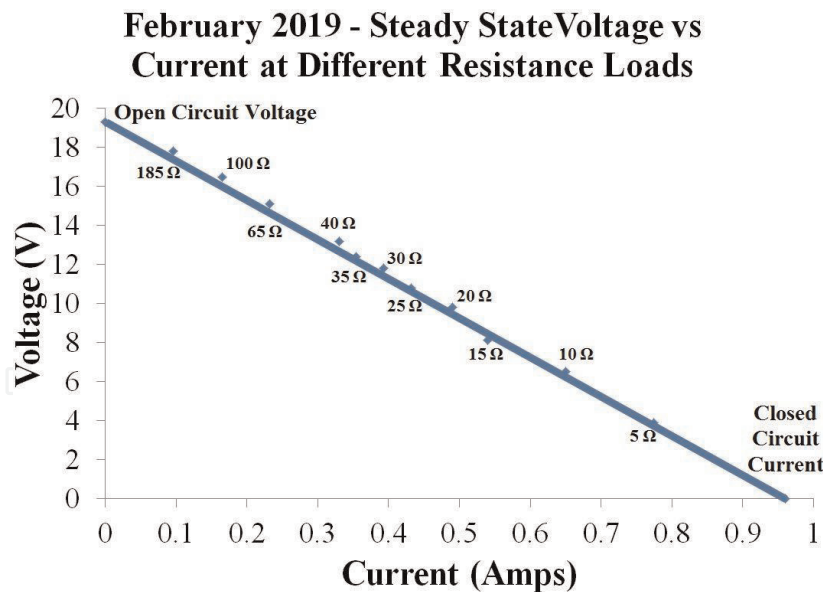


Figure 9.

Steady state voltage versus amperage linear relationship data from the New York City test bed recorded in February 2019.

6. Applications

A primary application of TEGs using passive cooling is in remote locations where normal powering methods for monitoring systems are problematic due to distance from the electrical grid. Where there are geothermal bore holes and steam pipes, the TEG described is a direct application and will function well, especially when ambient temperatures are low. In contrast, solar power options are weather dependent, limited during the winter months, and colder temperatures are detrimental to their stand-alone batteries.

Developments in mobile and handheld electronics have enabled low-power designs with new connectivity and energy-saving scenarios through incorporation of integrated circuits and microcontroller units. As the processing power of computers increased, the need for transferring and sharing information became stronger. Monitoring systems, which used to be run as stand-alone systems, are now networked with other systems. In many cases, these systems are also control systems. Information sharing provides a clearer overall picture of the process and allows for more intelligent control.

The need for real time data or simplified data collection from multiple sensors has driven the development of wired and wireless sensor solutions. In the case of wired connections, the need for an external power supply is often eliminated by enabling the sensors to function as parasites and draw their power from the data line. Power for running wireless systems is normally obtained from either batteries or internal power supplies. The advances in both low-power electronics and ambient energy harvesting have led to significant industrial and academic research on wire- and battery-free sensors and devices. Wireless sensors powered by ambient energy can be found in transportation, building automation, industry, and other applications. This technology eliminates the need to buy and replace batteries, and units can be left unattended in hazardous or difficult-to-get-to places.

The authors have developed an intensive open-field heat agriculture system using geothermal steam and steam condensate that extends growing seasons and enables the cultivation of out-of-region, non-native crops [31, 32]. It has an underground piping system in Iceland that is similar to the method for heating sidewalks and how waste heat from combined heat and power (CHP) systems warm green

roofs [33]. The TEG described herein has been used to power automated irrigation systems [34], robotic remote monitoring systems [35], and a series of web-accessible security cameras working on both LAN and 3G wireless networks in New York City and Iceland, respectively [36–39].

7. Conclusions

The passive TEG described has no moving parts and relies on ambient air cooling. It can maintain a temperature difference (ΔT) across a series of TEMs of 76°C. In one iteration, it produces 6.9 W of steady state power with 31.2 V open circuit and 0.89 A short circuit. Successful applications include powering two microcontroller-based security cameras, one with a wireless Local Area Network (LAN) and another with cellular connectivity, as well as LED lights, a cellular-interfaced video surveillance system, and monitoring robots, while simultaneously trickle charging batteries. The most recent application was to power a complete 3G wireless security network. Future work includes optimizing the cold block to further increase the ΔT across the TEMs.

Acknowledgements

The authors acknowledge the support extended by the following organizations, institutions and corporations: The Cooper Union for the Advancement of Science and Art, the Center for Innovation and Applied Technology, the Agricultural University of Iceland, the University of Iceland, Arvirkinn ehf, Timtronics, the City of Hveragerdi, and Keilir Institute of Technology. Special thanks to: Gudmundur Gislason, Ruth Nerken, Mark Epstein, Barry Shoop, Richard Stock, Anita Raja, Melody Baglione, George Sidebotham, Chih S. Wei, Gudridur Helgadóttir, Aldis Hafsteinsdóttir, Elias Oskarsson, Borkur Hrafnkelsson, Mar Gudmundsson, Fridrik Brekkan, Stefan Sigurdsson, Gísli Páll Pálsson and Aladino Melendez. The authors acknowledge the contributions of the Center for Innovation and Applied Technology Research Assistants: Daniel Abes, Jeahoung Hong, Seung Won Na, Jabin Pu, Christopher E, Jing Jin, Sanjev Menon, Di Yi Liu, Daniel Feyman, Alinur Rahim, Justin Jose, James Ngai, Hou Chong Chan, Issei Abraham Yamada, Wei Yan Tin, Chengyin Jiang, Yueyue Li, TaeKoung Lee, Harrison Milne, Romaniya Voloshchuk, Monica Chen, Jordan Selig, and Matthew Cavallaro.

Conflict of interest

The authors declare no conflict of interest. The founding sponsors had no role in the design of the study; in the collection, analyses, or interpretation of data; in the writing of the manuscript, and in the decision to publish the results.

Nomenclature

Δ	change
∇	gradient
α	Seebeck coefficient
A_{hb}	hot block effective surface area
A_s	steam effective surface area
A_p	pipe effective surface area

h_s	steam convective coefficient
I	current
I_c	short circuit current
I_L	load current
k_{hb}	hot block thermal conductivity
k_p	pipe thermal conductivity
n_m	number of TEMs in the array
N	number of fins
P_L	load power
r_i	internal resistance
r_L	load resistance
R_C	cold block thermal resistance
$R_{contact}$	contact thermal resistance
R_{fin}	fin thermal resistance
R_h	fin convective thermal resistance
R_H	hot block system thermal resistance
$R_{hotblock}$	hot block thermal resistance
R_k	fin conductive thermal resistance
R_m	TEM thermal resistance
R_{TEM}	TEM array thermal resistance
R_{steam}	steam thermal resistance
R_{pipe}	pipe thermal resistance
t_{hb}	hot block average thickness
t_p	pipe wall thickness
T	temperature
T_c	hot side temperature
T_h	cold side temperature
V	voltage
V_o	open circuit voltage
V_L	load voltage

Author details


Robert Dell^{1*}, Michael Thomas Petralia¹, Ashish Pokharel¹ and Runar Unnthorsson²

¹ Center for Innovation and Applied Technology, Mechanical Engineering, The Cooper Union, New York, NY, USA

² Faculty of Industrial Engineering, Mechanical Engineering, and Computer Science, University of Iceland, Reykjavik, Iceland

*Address all correspondence to: rdell@cooper.edu

IntechOpen

© 2019 The Author(s). Licensee IntechOpen. This chapter is distributed under the terms of the Creative Commons Attribution License (<http://creativecommons.org/licenses/by/3.0>), which permits unrestricted use, distribution, and reproduction in any medium, provided the original work is properly cited. 

References

- [1] Ioffe A. Semiconductor Thermoelements and Thermoelectric Cooling. London: Infosearch Limited; 1957. 184 p
- [2] Pollock D. Thermocouples: Theory and Properties. Boca Raton: CRC Press, Inc.; 1991. 336 p LCCN: 91-24377
- [3] Aepinus F. Tentamen Theoriae Electricitatis et Magnetism. Petropoli: Typis Academiae Scientiarum; 1759. 390 p
- [4] Home R. Aepinus, the tourmaline crystal, and the theory of electricity and magnetism. *Isis*. 1976;1:21-30. DOI: 10.1086/351542
- [5] Goupil C et al. Thermodynamics and thermoelectricity. In: Goupil C, editor. *Continuum Theory and Modeling of Thermoelectric Elements*. Weinheim: Wiley-VCH; 2015. pp. 1-73. DOI: 10.1002/9783527338405.ch1
- [6] Volta A. Nuova memoria sull'elettricità animale, divisa in tre lettere, dirette al signor abate Anton Maria Vassalli Lettera prima. *Annali di Chimica e Storia Naturale*. 1794;5: 132-144
- [7] Wikipedia, Thermoelectric effect: Note 1 [Internet]. 2019. Available from: https://en.wikipedia.org/wiki/Thermoelectric_effect [Accessed 2019-01-09]
- [8] Seebeck T. Über den Magnetismus der Galvanischen Kette. Berlin: der Königlichen Akademie der Wissenschaft; 1822. 58 p
- [9] Oersted M. Nouvelles expériences de M. Seebeck sur les actions électromagnétiques. *Annales de Chimie et de Physique*. 1823;22:199-201
- [10] Oersted M. Notiz von neuen electrisch-magnetischen Versuchen des Herrn Seebeck in Berlin. *Annalen der Physik*. 1823;73:430-432
- [11] Seebeck T. Magnetische polarisation der metalle und erze durch temperatur-differenz. *Abhandlungen der Königlichen Akademie der Wissenschaften zu Berlin*. 1825:265-373. <https://books.google.com/books?id=E27NAAAAMAAJ&pg=PA265#v=onepage&q&f=false>
- [12] Seebeck T. Ueber die magnetische polarisation der metalle und erze durch temperatur-differenz. *Annalen der Physik und Chemie*. 1826;6:1-20, 133-160, 253-286
- [13] Goldsmid H. *Introduction to Thermoelectricity*. 2nd ed. Berlin: Springer-Verlag; 2016. 278 p. DOI: 10.1007/9783662492567
- [14] Peltier J. Nouvelles expériences sur la caloricité des courants électrique. *Annales de Chimie et de Physique*. 1834; 56:371-386
- [15] Thomson W. On a mechanical theory of thermo-electric currents. *Proceedings of the Royal Society of Edinburgh*. 1851;42:91-98
- [16] Heikes R, Ure R. *Thermoelectricity: Science and Engineering*. New York: Interscience Publishers, Inc.; 1961. LCCN: 61-9650
- [17] Harman T, Honig J. *Thermoelectric and Thermomagnetic Effects and Applications*. New York: McGraw-Hill, Inc.; 1967 LCCN: 66-20717
- [18] Tian Z, Lee S, Chen G. Comprehensive review of heat transfer in thermoelectric materials and devices. *Annual Review of Heat Transfer*. 2014;17:425-483. DOI: 10.1615/AnnualRevHeatTransfer.2014006932
- [19] Zhang X, Zhao L. Thermoelectric materials: Energy conversion between

heat and electricity. *Journal of Materiomics*. 2015;1:92-105. DOI: 10.1016/j.jmat.2015.01.001

[20] Ge Z et al. Low-cost, abundant binary sulfides as promising thermoelectric materials. *Materials Today*. 2016;4:227-239. DOI: 10.1016/j.mattod.2015.10.004

[21] LeBlanc S. Thermoelectric generators: Linking material properties and systems engineering for waste heat recovery applications. *Sustainable Materials and Technologies*. 2014;1-2: 26-35. DOI: 10.1016/j.susmat.2014.11.002

[22] Paul D. Thermoelectric energy harvesting. In: Fagas G, Gammaitoni L, Paul D, editors. *ICT–Energy–Concepts Towards Zero: Power Information and Communications Technology*. London: Intech; 2014. 49-78 p. DOI: 10.5772/55410

[23] Lawrence Livermore National Laboratory, *Energy Flow Charts: Estimated U.S. Energy Consumption in 2017: 97.7 Quads* [Internet]. 2019. Available from: https://flowcharts.llnl.gov/content/assets/docs/2017_United-States_Energy.pdf [Accessed: 2019-01-09]

[24] Lee H. *Thermal Design: Heat Sinks, Thermoelectrics, Heat Pipes, Compact Heat Exchangers, and Solar Cells*. Hoboken: John Wiley & Sons, Inc.; 2010. 2 p. DOI: 10.1002/9780470949979

[25] Çengel Y, Boles M. *Thermodynamics: An Engineering Approach*. 4th ed. New York: McGraw-Hill; 2002. 275. p 10:0072383321

[26] Goupil C et al. Thermodynamics of thermoelectric phenomena and applications. *Entropy*. 2011;13: 1481-1517. DOI: 10.3390/e13081481

[27] Dell R, Wei S, Sidebotham G. Thermoelectric Power Generation

Device. European Patent No. EP 2,095,440 B1, U.S. Patent No. US 8,829,326 B2, and 9,590,160, Canadian Patent No. CA 2,671,995, 7 March 2017

[28] Dell R et al. A thermoelectric-based point of use power generator for steam pipes. *Geothermal Resources Council Transactions*. 2011;35:1237-1241

[29] Dell R et al. Thermoelectric-based power generator for powering microcontroller based security camera. In: *Proceedings of the ASME 2012 International Mechanical Engineering Congress and Exposition (IMECE2012)*; 9–15 November 2012. Houston, USA: IMECE; 2012. pp. 635-642. DOI: 10.1115/IMECE2012-89611

[30] Sidebotham G. *Heat Transfer Modeling*. Cham: Springer; 2015. viii p. DOI: 10.1007/9783319145143

[31] Dell R et al. Repurposing waste steam and hot water to accelerate plant growth in heated green roofs. In: *Proceedings of the ASME 2013 International Mechanical Engineering Congress and Exposition (IMECE2013)*; 15-21 November 2013. San Diego, USA: IMECE; 2013. DOI: 10.1115/IMECE2013-65200

[32] Dell R et al. Waste geothermal hot water for enhanced outdoor agricultural production. In: *Proceedings of the ASME 2013 Power Conference (POWER2013)*; 29 July–August 1 2013. Boston, USA: POWER; 2013. DOI: 10.1115/POWER2013-98172

[33] Dell R et al. Geothermal heat in agriculture: Preliminary results of an energy intensive system in Iceland. *Geothermal Resources Council Transactions*. 2011;35:115-121

[34] Foley W et al. Point of use thermoelectric powered automated irrigation system for an intensive shallow bottom heat system using waste geothermal hot water and steam

condensate in Iceland. Geothermal Resources Council Transactions. 2015; **39**:117-123

[35] Dell R et al. A thermoelectric powered quadruped robotic system for remote monitoring of geothermal open field heated gardens in Iceland. Geothermal Resources Council Transactions. 2016;**40**:173-180

[36] Dell R et al. Web accessible security camera system independently powered by a point of use thermoelectric generator using geothermal pipes as a heat source. Geothermal Resources Council Transactions. 2014;**38**:729-733

[37] Dell R et al. A web-accessible robotics monitoring system powered by a thermoelectric generator connected to a battery. In: Proceedings of the ASME 2014 International Mechanical Engineering Congress and Exposition (IMECE2014); 14-20 November 2014. Montreal, Quebec: IMECE; 2014. DOI: 10.1115/IMECE2014-39077

[38] Dell R et al. 3G security camera network using a thermoelectric generator powered by a geothermal steam pipe in Iceland. Geothermal Resources Council Transactions. 2017; **41**:691-703

[39] Dell R et al. Thermoelectric powered security systems in Iceland using a geothermal steam pipe as a heat source. Proceedings. 2018;**2**:440. DOI: 10.3390/ICEM18-05309